

Time-of-Flight Signatures of Bosons in a Double Well

Analabha Roy and L.E. Reichl
Center for Complex Quantum Systems
and

Department of Physics
The University of Texas at Austin, Austin, Texas 78712

November 15, 2018

Abstract

We present analytical and numerical treatments for evaluating the time-of-flight momentum distribution for the stationary states of a two-boson system trapped in a quartic double-well potential, paying particular attention to the Tonks and noninteracting regimes. We find that the time-of-flight distributions can serve as a valuable tool in profiling the states of this system, which will be useful in understanding the chaotic dynamics of coherent quantum controlled excitations of trapped bosons.

1 Introduction

The study of ultracold boson systems in Optical Dipole Traps (ODT) such as Bose-Einstein condensates, have received considerable attention in academia in the last three decades [1] [2] [3] [4]. More recently, experiments involving number squeezed states of trapped alkali atoms have yielded promise [5]. New techniques, such as quantum tweezing [6] and quantum many-body culling [5], are being developed that can create mesoscopic two-boson systems out of ultracold atoms in optical traps. Theoretical studies demonstrate the possibility of number state generation by atomic culling as well [7]. Such a two-boson system can be subjected to a micrometer-scale double well by various means, ranging from Gaussian lasers [8], to small volume optical traps [5]. An optical lattice of such double-wells can also be generated by two counter-propagating lasers of linearly polarized light with a known angle between their planes of polarization, and a transverse magnetic field to mix the two potentials [9]. If the on-site lattice depth is sufficiently deep then the tunneling between the sites can be neglected. Furthermore, if they are loaded homogeneously from a cold-atom system confined in an optical dipole trap by number squeezing, followed by adiabatically reducing the laser intensity so that the distribution in each site is

culled down to the subpoissonian regime ($N=2$ per site) [5], each double well system can be treated in isolation exactly as depicted in [10].

This system can then be excited to higher energies using stimulated Raman scattering. As we have shown [10], coherent population transfer from the ground state into one of the excited states can be achieved using time-modulated (ie pulsed) radiation pulses. If the time scale of the pulse modulation is sufficiently large, the Raman process is adiabatic (called Stimulated Raman Adiabatic Passage or STIRAP) [11]. The presence of avoided crossings contributed by resonating levels other than the ones that the radiation pulses connect have been predicted [10]. These avoided crossings in the Floquet eigenphases appear due to level repulsion caused by a loss of symmetry/degeneracy (actual crossings) [12], and affect the statistical properties of the spectra, bringing them close to that predicted by random matrix theory. These are connected with the dynamics of the underlying classical system, which undergo a transition from KAM tori to chaos in this region of the parameter space [12]. Thus, this system can be used to demonstrate the quantum effects of chaos, induced by the radiation, on multilevel transitions in a 2-boson system.

In the following sections, we evaluate the time of flight (tof) signatures of these wavefunctions, and discuss the extent to which they are useful in observing chaos. Section 2 details how the double well system was diagonalized and the eigenfunctions obtained. Section 3 we discuss the nature of the time-of-flight signatures of the different states, and display our numerical results in section 4. Concluding remarks are made in the final section.

2 The Eigensystem

Our system consists of two alkali metal bosons confined to a double-well optical potential. The effective interaction between the bosons, in three dimensions, is obtained in the long wavelength approximation to be

$$u^{3d}(\mathbf{x}_1 - \mathbf{x}_2) = \frac{4\pi\hbar^2 a_s}{m} \delta(\mathbf{x}_1 - \mathbf{x}_2), \quad (1)$$

where \hbar is Planck's constant, a_s is the s-wave scattering length and $\mathbf{x}_i = (x_i, y_i, z_i)$ is the displacement of the i th particle [13] [14]. The system can be confined in two spacial (radial) directions so that the essential dynamics occurs in the x - direction by the use of anisotropic magnetic traps with high aspect ratio [15] [16]. In that case, the other 2 dimensions can be integrated out [10] [15], yielding an effective 1-dimensional interaction

$$u(x_1 - x_2) = 4a_s\omega_s\hbar\delta(x_1 - x_2) \quad (2)$$

We will consider the case of two identical bosons confined to a quartic double well potential. We get the total Hamiltonian for the system to be

$$H = p_1^2 + p_2^2 + V_0(-2x_1^2 + x_1^4) + V_0(-2x_2^2 + x_2^4) + U_0\delta(x_1 - x_2). \quad (3)$$

where p_i is the momentum of the i th particle ($i=1,2$), x_i is the position of the i th particle along the x-axis, and V_0 determines the depth of the double well potential. We have used dimensionless expressions for all the degrees of freedom, as well as the system parameters, by introducing a characteristic length scale L_u . Thus, the actual Hamiltonian H' relates to the dimensionless Hamiltonian H as $H = \frac{H'}{E_u}$, where $E_u = \frac{\hbar^2}{2mL_u^2}$. Similarly, $U_0 = \frac{4a_s\omega_s\hbar}{E_u}$ and the time scales as $t = \frac{t'}{T_u}$ where $T_u = \frac{2mL_u^2}{\hbar}$. Fig. 1 shows a plot of the quartic double well $V(x) = V_0(-2x^2 + x^4)$ for well depth $V_0 = 7.2912229$.

The numerical diagonalization of the Hamiltonian in Eq. (3) is facilitated by a nonadaptive finite element method using the analytically obtained matrix elements of the Hamiltonian in a finite wave train basis of size $L = 3.5$ (in units of L_u),

$$\langle x_1, x_2 | n_1, n_2 \rangle^{(s)} = \frac{1}{\sqrt{2(1 + \delta_{n_1, n_2})}} [\langle x_1 | n_1 \rangle \langle x_2 | n_2 \rangle + \langle x_1 | n_2 \rangle \langle x_2 | n_1 \rangle]. \quad (4)$$

Here,

$$\langle x | n \rangle = \frac{1}{\sqrt{L}} \sin \left[\frac{n\pi}{2} \left(\frac{x}{L} - 1 \right) \right] \quad (5)$$

within the range $-L \leq x \leq L$ and vanishes outside.

We will investigate the tof distributions in two regimes of the (V_0, U_0) parameter space. The first regime, henceforth referred to as the 'Tonks regime' will consist of a very strongly repulsive system and a moderate well depth. We define the 'Tonks Factor' for this system, γ , as

$$\gamma \equiv \frac{U_0}{J}. \quad (6)$$

Here, J , the zero point fluctuation, is a measure of the ability of the ground state bosons to tunnel across from one well to another. When $\gamma \rightarrow \infty$, we reach the 'Tonks Gas' regime where the particles are essentially Fermionic, and the interaction completely dominates the system [17]. Fig 2 shows the evolution of the ground state of the system as γ is increased. The order parameter being plotted as a function of γ ,

$$\psi \equiv \int dx |\langle x_1 = x_2 | E_1 \rangle|^2, \quad (7)$$

is the total probability that the two particles will be together. As expected, it vanishes for arbitrarily large values of γ , where the particles assume Fermionic characteristic, since no two particles can occupy the same position. The transition to this regime is not consistent, however. We note 4 distinct ranges of γ for which the decay rates of ψ are different. In the first three ranges, the decay rate seems to be exponential ie $\psi_i = \psi_i^0 e^{(-\gamma/\gamma_i^0)}$ for $i = 1, 2, 3$. The data points have been fitted to exponents by the use of numerical nonlinear least-squares algorithms. The decay rate, characterized by γ_i^0 , decreases sharply at $\gamma \sim 1, 2$ and 6. Near $\gamma \sim 7$, there is a sharp increase in ψ after which it continues to

decrease. If we neglect the probability if it falls below $1/e$ of the maximum, then the 'Tonks regime' is achieved beyond $\gamma \sim 0.4$. In our case, we have chosen a γ of 5.20142 for our Tonks regime, placing the system in region 3 of Fig 2. The value of (V_0, U_0) chosen is $(4.0, 40.0)$.

The second regime, henceforth referred to as the 'Single particle regime', will consist of a weakly attractive system and the well-depth as seen in [10]. Thus, the parameter values chosen are $(7.2912229, -1.0)$.

The probability distributions of the ground state $|E_1\rangle$, as well as the excited states $|E_2\rangle$ and $|E_4\rangle$, given by Eq 3 are shown in figs 3.a through 3.c for the Tonks regime. Note that, as expected, the states have distinct fermionic characteristics where there is virtually no probability that $x_1 = x_2$.

The probability distributions of the first seven quantum energy states of the system in the single particle regime are shown in figs. 4.a through 4.g. Note the plots of the ground state, $|E_1\rangle$, third excited state, $|E_4\rangle$, and sixth excited state $|E_7\rangle$. The dynamics of the system, when driven by sequential pulses whose energies are tuned to transitions between these states, show the effects of dynamical chaos through level-repulsion in the Floquet eigenphases [10]. A crossing through the level-repelling region can be avoided if the radiation pulses are applied adiabatically, producing a chaos assisted passage as detailed in [10].

3 Time of Flight Images

The normalized first order correlation function of a single double well is a measurement of the atomic density $n(x)$. Such correlations can be measured following a STIRAP transition by the time-of-flight (TOF) technique in which the trapped atoms are released sufficiently quickly that the diabatic approximation in quantum mechanics can be applied. The atoms then expand ballistically until they reach a detection plate. If the plate is far enough from the double well system that the far-field approximation can be used, then the Green's Function for the system can be simplified and the time translation reduced to a simple Fourier Transform. Thus, for a time-of-flight τ , an atom initially localized at lattice site i in the state $\Phi(x' - x'_i, t' = 0)$ becomes [18]

$$\Psi(x, \tau) = \sqrt{\frac{-i}{4\pi\tau}} \exp \left[i \frac{1}{2\tau} \left(\frac{x^2}{2} + xx'_i \right) \right] F[\Phi(x')]_{u=\frac{x}{4\pi\tau}}, \quad (8)$$

where the primed coordinates refer to the optical system, the unprimed coordinates refer to the detector, and u is the reciprocal lattice. The relation between the detector-lattice separation L and the time-of-flight τ is given by the ballistic de-Broglie equation

$$L^2 = \tau \frac{h}{m}. \quad (9)$$

For a large collection of such systems, each in the desired pure state, the measured TOF is simply the probability obtained from Eq. 8 times the number

of such double wells N (which we shall subsequently drop off as an appropriately adjusted overall normalization).

$$n(x) = N \frac{1}{4\pi\tau} |F[\Phi(x')]_{u=\frac{x}{4\pi\tau}}|^2 \quad (10)$$

We note that there are noticeable differences in the symmetries of the two states $|E_4\rangle$ and $|E_7\rangle$ (refer to Figs that are the two possible outcomes of STIRAP in this system. The distinctly resolved peaks in each wavefunction (labeled 1 through 8 for $|E_7\rangle$) can be approximated by elliptical Gaussian functions. Thus, the wavefunction can be represented by a two-dimensional function as follows:

$$\Phi(x'_1, x'_2) = \sum_{i=1}^R a_i G(x'_1, x'_1, \alpha_1^i) G(x'_2, x'_2, \alpha_2^i), \quad (11)$$

where

$$G(x, x^i, \alpha) = \left(\frac{2\alpha}{\pi}\right)^{1/4} e^{-\alpha(x-x^i)^2}. \quad (12)$$

Here, R is the number of peaks (8 for $|E_7\rangle$). Also, we have rotated our coordinate system to the axes of symmetry (by 45 degrees) of $|E_7\rangle$. Using the well-known relation for the Fourier transform of a Gaussian applied to Eqns 10 and 11, we get (sans any overall normalizations),

$$n(x_1, x_2) = \left| \sum_{j=1}^R a_j \left(\frac{1}{4\pi^2 \alpha_1^j \alpha_2^j} \right)^{1/4} e^{i \frac{x_1 x_1^j + x_2 x_2^j}{4\pi\tau}} e^{-\frac{x_1^2}{16\pi^2 \alpha_1^j \tau^2}} e^{-\frac{x_2^2}{16\pi^2 \alpha_2^j \tau^2}} \right|^2. \quad (13)$$

We rewrite this as

$$n(x_1, x_2) = \left| \sum_{j=1}^R r_j(x_1, x_2) e^{ik_j x_1} \right|^2 \quad (14)$$

$$r_j(x_1, x_2) = a_j \left(\frac{1}{4\pi^2 \alpha_1^j \alpha_2^j} \right)^{1/4} e^{i \frac{x_2 x_2^j}{4\pi\tau}} e^{-\frac{x_1^2}{16\pi^2 \alpha_1^j \tau^2}} e^{-\frac{x_2^2}{16\pi^2 \alpha_2^j \tau^2}} \quad (15)$$

$$k_j = \frac{x_1^j}{4\pi\tau} \quad (16)$$

The expression above can be simplified to

$$n(x_1, x_2) = \sum_{j=1}^R |r_j(x_1, x_2)|^2 + \sum_{\langle i, j \rangle} 2r_i^*(x_1, x_2) r_j(x_1, x_2) |\cos(k_j - k_i)x| \quad (17)$$

In order to get the density functional $n(x)$, we integrate out the x_2 (symmetries guarantee that the result will be the same if we integrate x_1 instead) and get

$$n(x) = \sum_{j=1}^R r_j^2(x) + \sum_{\langle i,j \rangle} 2r_{ij}^2(x) |\cos(k_j - k_i)x| \quad (18)$$

where $\langle i, j \rangle$ are distinct (ie $i \neq j$) combination pairs of peaks. In the equation above, integrating x_2 by Gaussian integral methods leaves out a Gaussian dependencies in x of r_j and r_{ij} (the subscripts for x have been dropped). Thus,

$$r_j^2(x) = \tau a_j^2 \sqrt{\frac{4\pi}{\alpha_1^j}} e^{-\frac{x^2}{16\pi^2 \alpha_1^j \tau^2}} \quad (19)$$

$$r_{ij}^2(x) = 2\tau a_i a_j \left(\frac{1}{\alpha_1^i \alpha_1^j \alpha_2^i \alpha_2^j} \right)^{\frac{1}{4}} \sqrt{\pi \alpha_2^{ij}} e^{-\frac{\alpha_2^{ij} (x_2^j - x_2^i)^2}{4}} e^{-\frac{x^2}{16\pi^2 \alpha_1^{ij} \tau^2}} \quad (20)$$

$$(21)$$

where we have defined

$$\frac{1}{\alpha^{ij}} = \frac{1}{\alpha^i} + \frac{1}{\alpha^j} \quad (22)$$

From the plot of $|E_7\rangle$ for the single particle regime (see Fig 4), we notice that there are only three distinct kinds of peaks (labeled 1, 5 and 8). Thus there are three pairs whose k 's are unequal viz. $\langle 1, 5 \rangle$ and $\langle 1, 8 \rangle$ and $\langle 5, 8 \rangle$. All other terms are absorbed into the perfect square terms in Eqn. 18. Each such term is a Gaussian centered at $x = 0$ with varying widths. If we look at values of x sufficiently far from the center of the detector plate, those terms drop off quickly, leaving just the three oscillatory terms. This signal will be distinct from that obtained from the TOF of state $|E_4\rangle$, which has only 2 such term (only 2 distinct kinds of peaks). If the time-of-flight τ is chosen so that the values of $k_j - k_i$ are small, then the signal will look like an amplitude modulated sinusoid. Since the transition to $|E_4\rangle$ is a chaotic, and the transition to $|E_7\rangle$ is caused by a chaos assisted adiabatic passage, the amplitude modulation differentiates between the two outcomes. In case there is an incoherent excitation, there will be large numbers of overlapping or closely spaced peaks and the oscillations will constructively interfere everywhere, thus distinguishing the resultant signal from one obtained by the TOF of a coherent excitation.

4 Time-of-Flight: Numerical Plots

Numerical results for the tof distributions of the eigenstates obtained in the previous section are shown in Figs 5 6. The distributions were evaluated using the nonadaptive finite-element-method using the same finite wave train basis that was used to numerically diagonalize the Hamiltonian in Eq 3 [10]. The Fourier transform of the finite wave train in Eqn 5 is given by

$$F[\langle x'|n\rangle] = \frac{1}{\sqrt{2L\pi}} \frac{1}{\left(\frac{n^2\pi^2}{4L^2} - u^2\right)} \left[2u \sin \frac{n\pi}{2} - \frac{n\pi}{L} \sin Lu \right] \quad (23)$$

Thus, a numerical expression for Eq 10 was obtained for two degrees of freedom x_1 and x_2 , and the density functional $n(x)$ determined by integrating out one of the coordinates by adaptive Gauss-Kronrod quadrature. The distributions are shown for tof $\tau = 10^5$ units of T_u . All the dynamics is essentially zero dimensional, and is independent of the length scale. For practical reasons, we choose an L_u of 50 nm [10]. Consequently, with a Rubidium-85 atomic mass of $85.4678 \text{ gmol}^{-1}$, we get a T_u of about $6.7 \mu s$, which makes τ to be 0.67 seconds. Using Eqn 9, we get a detector distance of about 2.2 cm.

Figs 5(a) through (c) show the tof distributions of the states $|E_1\rangle$, $|E_2\rangle$, and $|E_4\rangle$ respectively for the Tonks gas detailed in section 1. Note that the momentum distribution of $|E_1\rangle$, closely approximates the Heavyside function that is characteristic of Fermions (barring the lack of any occupancy at zero momentum, which is forbidden in this case due to the zero point fluctuation J).

Figs 6(a) through (c) show the tof distributions of the states $|E_1\rangle$, $|E_4\rangle$, and $|E_7\rangle$ respectively in the single particle regime detailed in section 1. Note that, as predicted by the calculations in section 3, the number of distinct oscillations in each distribution correspond to the number of distinct pairs of peaks seen in the wavefunctions. Thus, each state generates a particular signature in the tof, and the presence of chaos can be determined by the one extra oscillation in Fig 6(c) compared to Fig 6(b).

Time of flight fluorescence methods for profiling the wavefunction, such as measuring the momentum distribution by interrupting the particle flow with counter-propagating laser beams and then measuring fluorescence as a function of time (time of flight absorption) [19] [20], will have high signal to noise ratio (compared to absorption) [5]. Single shot fluorescence images should duplicate the profile shown in Figures 6(a)-(c).

5 Conclusions

We have obtained and analyzed the time-of-flight images of a two-boson system subjected to optical double well potentials. The tof plots help in distinguishing the different outcomes of STIRAP excitations of such systems, depending on the time scales of the driving radiation pulses. The presence of chaos in these dynamics affect the outcome and influence the pattern that will be seen on the detector as extra oscillations in the spacial variation of fluorescence. These oscillations can be resolved by choosing an appropriately high value of τ which reduces the frequencies. The momentum probability distributions of the tof do not provide enough information to uniquely profile the original wavefunction spatially, since two neighboring states with opposite parities will provide nearly the same tof distribution. However, quantum control methods like STIRAP can be tuned to forbid those transitions, making tof a valuable tool in profiling the final states of quantum controlled excitations in cold atom systems.

6 Acknowledgments

The authors wish to thank the Robert A. Welch Foundation (Grant No. F-1051) for support of this work. A.R. thanks Prof. Mark Raizen for useful discussions about time-of-flight and the possibility of experiments on this system.

References

- [1] C. Monroe, W. Swann, H. Robinson and C. Wieman, Phys. Rev. Lett. **65**, 1571 (1990)
- [2] M. H. Anderson, J. R. Ensher, M. R. Matthews, C. E. Wieman and E. A. Cornell, Science **269**, 198 (1995)
- [3] W. Ketterle, K. B. Davis, M. A. Joffe, A. Martin and D. E. Pritchard, Phys. Rev. Lett. **70**, 2253 (1993)
- [4] K. B. Davis, M.-O. Mewes, M. R. Andrews, N. J. van Druten, D. S. Durfee, D. M. Kurn and W. Ketterle, Phys. Rev. Lett. **75**, 3969 (1995)
- [5] C.-S. Chuu, F. Schreck, T.P. Meyrath, J.L. Hansses, G.N. Price, and M.G. Raizen, Phys. Rev. Lett. , **95** 260403 (2005).
- [6] Roberto B. Diener, Biao Wu, Mark Raizen, and Qian Niu, Phys. Rev. Lett., **89** 070401 (2002).
- [7] A.M. dudarev, M.G. Raizen, and Qian Niu, Phys. Rev. Lett. , **98**, 063001 (2007)
- [8] Y. Shin, M. Saba, T. A. Pasquini, W. Ketterle, D. E. Pritchard, and A. E. Leanhardt, Phys. Rev. Lett., **92** 050405 (2004).
- [9] Ivan H. Deutsch and Poul S. Jessen, Phys. Rev. A **57**, 1972 (1998).
- [10] A. Roy and L.E. Reichl, Phys. Rev. A, **77**, 033418 (2008)
- [11] Nikolay V. Vitanov, Thomas Halfmann, Bruce W. Shore, and Klaas Bergmann, Annu. Rev. Phys. Chem., **52** 763 (2001).
- [12] L.E. Reichl, *The Transition to Chaos: Conservative Classical Systems and Quantum Manifestations, 2nd Edition*, Chapter 7, (Springer-Verlag, Berlin, 2004).
- [13] H.J. Metcalf and P. van der Straten, *Laser Cooling and Trapping*, (Springer-Verlag, New York, 1999)
- [14] C.J. Pethick and H.Smith, *Bose-Einstein Condensation in Dilute Gases*, (Cambridge University Press, Cambridge, 2002).
- [15] M. Olshanii, Phys. Rev. Lett., **81** 938 (1998).

- [16] D. S. Petrov, G.V. Shlyapnikov, and J. T. M. Walraven, Phys. Rev. Lett., **85** 3745 (2000).
- [17] Beln Paredes, Artur Widera, Valentin Murg, Olaf Mandel, Simon Flling, Ignacio Cirac, Gora V. Shlyapnikov, Theodor W. Hnsch, and Immanuel Bloch, Nature **429**, 277-281 (2004)
- [18] J. Grondalski, P.M. Alsing and I.H. Deutsch, Opt Expr, **5**, 11, 249 (1999)
- [19] Paul D. Lett, Richard N. Watts, Christif I. Westbrook, William.D Phillips, Phillip L. Gould, and Harold J. Metcalf, Phys Rev Lett. **61**, 2, 169 (1988)
- [20] <http://cold-atoms.physics.lsa.umich.edu/projects/lattice/T0F.html>

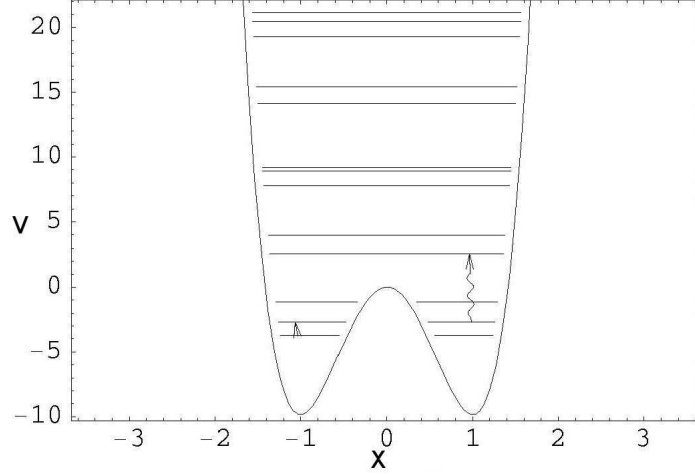


Figure 1: Plot of the double-well potential experienced by each boson. The energy levels, $E_1 = -6.42262$, $E_2 = -5.68883$ and $E_4 = 0.640055$ of the interacting two-boson system (interaction strength $U_0 = -1.0$) are also sketched, with wavy arrows denoting the levels connected by the STIRAP pulses. Note the slightly detuned resonance between the $2 \leftrightarrow 4$ and the $4 \leftrightarrow 7$ levels where $E_7 = 6.96998$. Here, $V_0 = 7.2912229$.

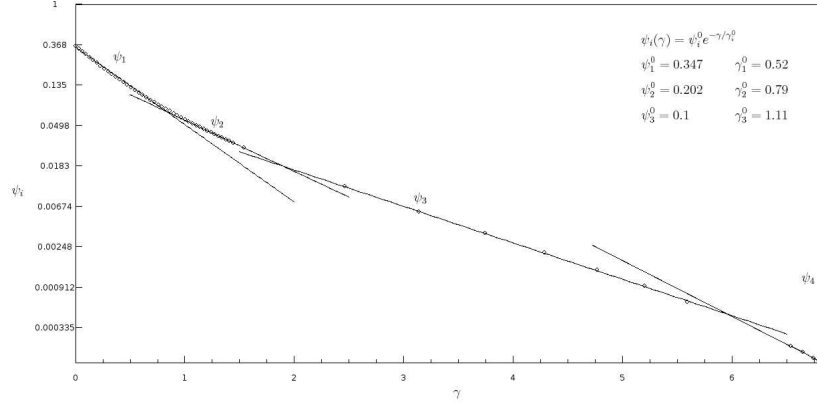


Figure 2: Semi-logarithmic plot of the probability ψ_i of two particles having the same position, as a function of the Tonks parameter γ for a constant $V_0 = 4.0$. The decay rate of ψ changes sharply at 4 regions, labeled by the index i . The data points (indicated by circles) have been fitted to exponential decay rates at each region (indicated by lines). The legend provides the numerically fitted values of the decay rates γ_i^0 . Note the discontinuous spike at $\gamma \sim 7$.

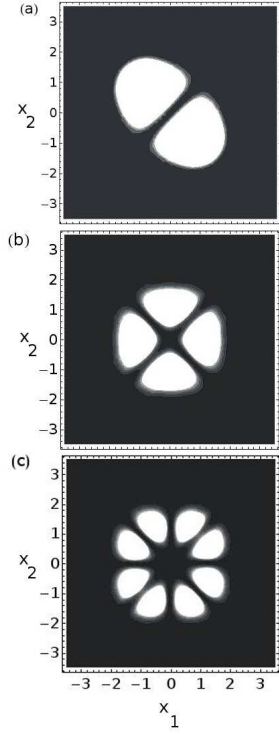


Figure 3: Plots of energy eigenfunctions for the two interacting bosons in a double well potential in the Tonks regime. Figures (a) through (c) are contour plots of the probability density $|\langle x_1, x_2 | E_1 \rangle|^2$, $|\langle x_1, x_2 | E_2 \rangle|^2$ and $|\langle x_1, x_2 | E_4 \rangle|^2$ respectively. The probabilities are plotted as functions of x_1 and x_2 . All units for all figures are dimensionless

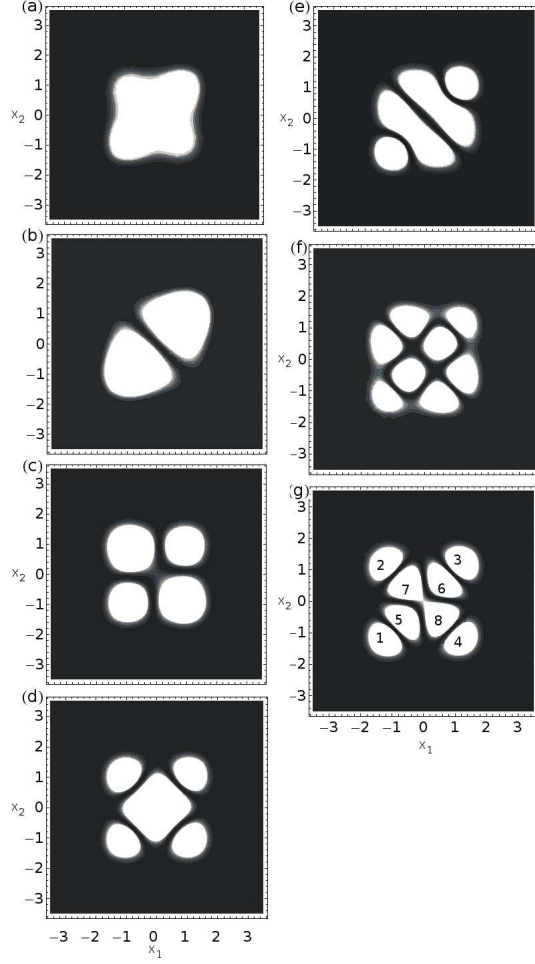


Figure 4: Plots of energy eigenfunctions for the two interacting bosons in a double well potential in the single particle regime. All units are dimensionless. Figures (a) through (f) are contour plots of the probability density $|\langle x_1, x_2 | E_1 \rangle|^2$ through $|\langle x_1, x_2 | E_6 \rangle|^2$ respectively. Figure (g) is a contour plot of the probability density $|\langle x_1, x_2 | E_7 \rangle|^2$. The peaks in the probability are numbered. The probabilities are plotted as functions of x_1 and x_2 . All units for all figures are dimensionless

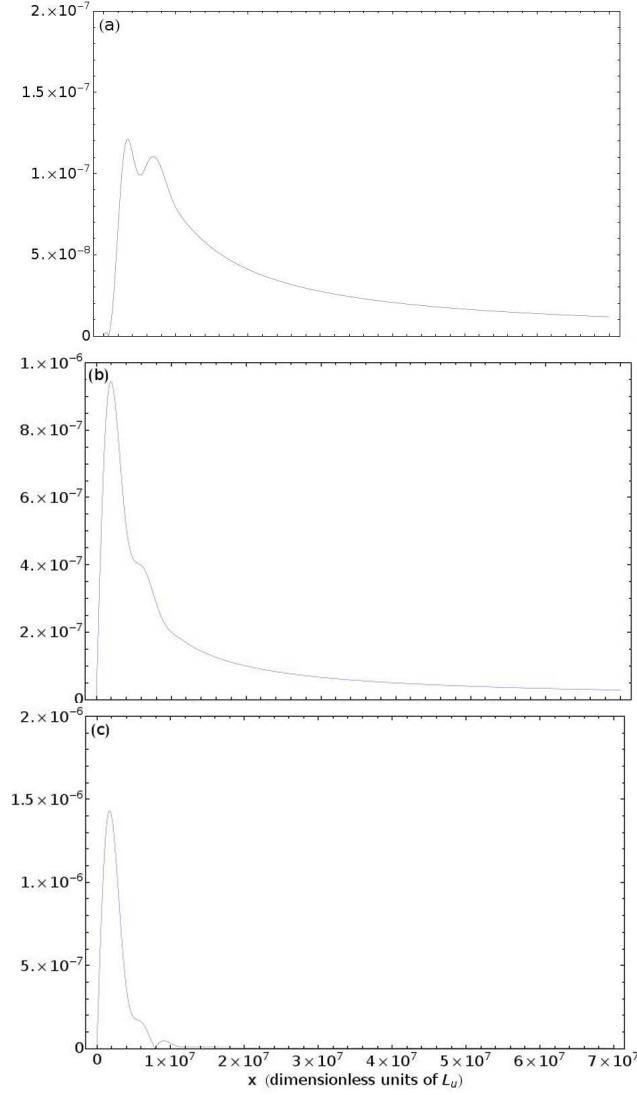


Figure 5: Figs (a) through (c) are plots of the one-dimensional time-of-flight distributions for the double-well eigenstates $|E_1\rangle$, $|E_4\rangle$ and $|E_7\rangle$ respectively in the Tonks regime. The distributions are symmetric about $x = 0$, so only the positive half is shown. The intensity $n(x)$ in the ordinate is for 10^6 double wells after a time of flight $\tau = 10^5$ (in units of T_u). The abscissa is shown in dimensionless units of L_u .

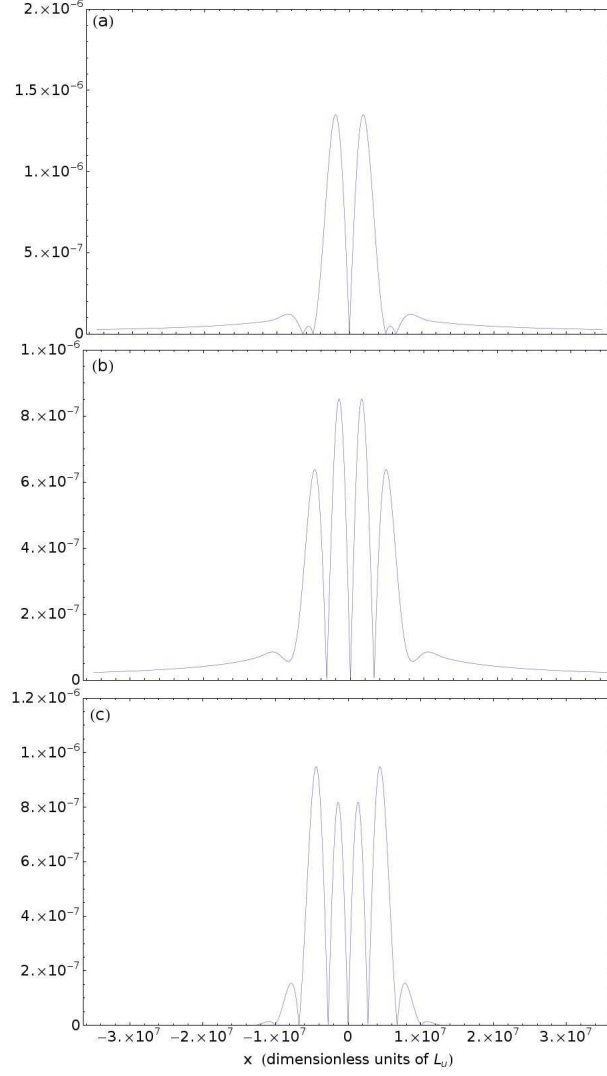


Figure 6: Figs (a) through (c) are plots of the time-of-flight distributions for the double-well eigenstates $|E_1\rangle$, $|E_4\rangle$ and $|E_7\rangle$ respectively in the single particle regime. The intensity $n(x)$ in the ordinate is for 10^6 double wells after a time of flight $\tau = 10^5$ (in units of T_u). The abscissa is shown in dimensionless units of L_u .